

Yield stress in metallic glasses: The jamming-unjamming transition studied through Monte Carlo simulations based on the activation-relaxation technique

David Rodney* and Christopher A. Schuh

Department of Materials Science and Engineering, Massachusetts Institute of Technology, Cambridge, Massachusetts 02139, USA
(Received 15 July 2009; revised manuscript received 11 September 2009; published 10 November 2009)

A Monte Carlo approach allowing for stress control is employed to study the yield stress of a two-dimensional metallic glass in the limit of low temperatures and long (infinite) time scales. The elementary thermally activated events are determined using the activation-relaxation technique (ART). By tracking the minimum-energy state of the glass for various applied stresses, we find a well-defined jamming-unjamming transition at a yield stress about 30% lower than the steady-state flow stress obtained in conventional strain-controlled quasistatic simulations. ART is then used to determine the evolution of the distribution of thermally activated events in the glass microstructure both below and above the yield stress. We show that aging below the yield stress increases the stability of the glass, both thermodynamically (the internal potential energy decreases) and dynamically (the aged glass is surrounded by higher-energy barriers than the initial quenched configuration). In contrast, deformation above the yield stress brings the glass into a high internal potential energy state that is only marginally stable, being surrounded by a high density of low-energy barriers. The strong influence of deformation on the glass state is also evidenced by the microstructure polarization, revealed here through an asymmetry of the distribution of thermally activated inelastic strains in glasses after simple shear deformation.

DOI: [10.1103/PhysRevB.80.184203](https://doi.org/10.1103/PhysRevB.80.184203)

PACS number(s): 62.20.F-, 83.60.La, 81.05.Kf

I. INTRODUCTION

The plasticity of metallic glasses is of fundamental interest for this emerging class of structural materials,¹ and also has broad relevance through analogy with other disordered systems, including colloidal,² granular,³ and fibrous⁴ materials, as well as emulsions and foams;⁵ a review spanning these various materials is provided in Ref. 6. All these systems have one important feature in common: at sufficiently high density and low temperature, they exhibit a stress-induced jamming-unjamming transition. Below a critical applied shear stress, the yield stress, they behave like solids (jammed) while above this stress, they flow like liquids (unjammed). The physical origin of the yield stress remains an open question of both fundamental and technological relevance.

Much insight has been obtained on the plasticity of metallic glasses through atomic-scale computer simulations. Glasses have been deformed either quasistatically by applying strain increments interspersed with energy minimizations^{7–20} or dynamically at constant strain-rates.^{21–30} It is important to note, however, that neither method accounts for thermally activated events. In quasistatic simulations, plastic events occur only when the glass is brought by the applied strain into positions of instability in the potential energy landscape,¹⁰ while dynamical simulations are strongly limited in time scale and thus require very high applied strain rates. Both simulation techniques are thus limited to regions of high internal shear stresses and are primarily relevant for fast deformation; while they may have some relevance for the propagation of shear bands,^{28,29} they do not apply to slower deformation, as in creep³¹ or aging.³²

Studying thermally activated processes requires a detailed characterization of the potential energy landscape of the system,³³ including its minima (the inherent structures)³⁴ and

saddle points (the activated states). Different methods to locate these configurations in glasses have been proposed, including excitation methods,^{35,36} basin-filling methods,^{37,38} and eigenvector-following methods.^{39–41} In the present article we employ a method from the third family, namely the activation-relaxation technique (ART), initially proposed by Mousseau and co-workers^{42–45} to study diffusion processes in glasses. In a previous article,⁴⁶ we used ART to reveal the energy landscape for deformation of a metallic glass. In that work, we showed that quasistatic shear deformation has a profound effect on the distribution of thermally activated events. In particular, the configurations reached during steady-state flow are surrounded by a high density of saddle points with low activation energies (<0.1 eV). They also have a specific microstructure, polarized by the applied shear deformation, as evidenced by an excess of thermally activated negative strain events after elastic unloading. These results underscore the highly nonequilibrium flow state attained in quasistatic simulations, and, by extension, in conventional molecular dynamics simulations.

In the present paper, we extend our prior work using ART to explore glass deformation, with the specific aim of revealing the structure and energy landscape of a glass deformed over long (infinite) time scales. Our approach is to use Monte Carlo simulations in conjunction with ART to identify the elementary thermally activated transitions at each step. In contrast to molecular dynamics or quasistatic simulations, we are able to effect true stress-controlled deformation for the first time in atomistic simulation, tracking as a function of applied stress the minimum-energy state of the glass, i.e., the configuration toward which the glass converges in the limit of long-time scales and low temperatures. We determine, with precision and without limitations due to thermal activation, the yield stress of the glass in this limit, and we directly observe the jamming-unjamming transition. Also, by

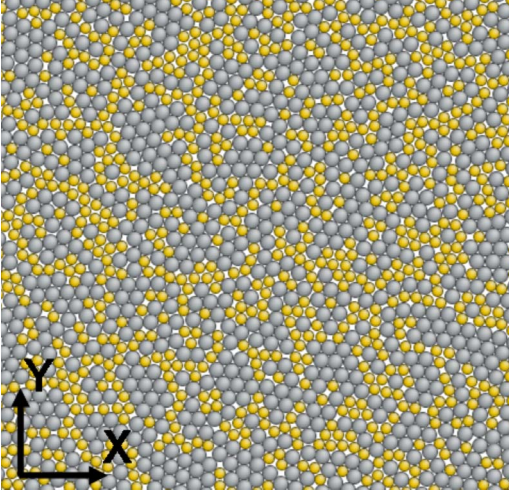


FIG. 1. (Color online) Atomic configuration of a glass. Copper atoms appear in yellow, zirconium atoms in gray. Only a section of the simulation cell is shown. The visualization software AtomEye (Ref. 50) was used.

using ART to sample the energy landscape around atomic configurations, we capture glass evolution both during aging below the yield stress and during shear flow above it.

II. METHODOLOGY

A. Atomic system and boundary conditions

We consider a two-dimensional (2D) binary equimolar glass made of $N=4000$ atoms that interact with the 8–4 Lennard-Jones potentials developed by Kobayashi *et al.*⁷ and already employed in Refs. 9, 47, and 48. An example section of a simulation cell is shown in Fig. 1. Periodic boundary conditions are used in both X and Y directions. A simple shear γ_{XY} is applied through Lees-Edwards periodic boundary conditions⁴⁹ by adding a shift $\Delta x = \gamma_{XY}L_Y$ along X between the upper and lower Y edges of the simulation cell.

An initial glass is obtained by quenching from a low-density gas at 2000 K with a cooling rate of 10^{11} K s⁻¹, using the Parrinello-Rahman algorithm^{51,52} to enforce zero average internal stresses. Below, we report all stresses normalized by the shear modulus of this glass, $\mu = 0.215$ eV/Å². After the initial quench, the cell dimensions L_X and L_Y are kept constant throughout the simulations.

B. Stress-controlled energy minimization

Conventional quasistatic shear simulations employ strain-controlled boundary conditions; the shift Δx between upper and lower Y edges is increased in small increments and the internal potential energy is minimized between increments at fixed applied strain. Although the present paper does not focus on such quasistatic simulations, we show in Fig. 2, as a reference for further comparison, the resulting variations of average internal shear stress and potential energy obtained in this way with the present system, starting from the initial quenched glass with strain increments of 10^{-4} .

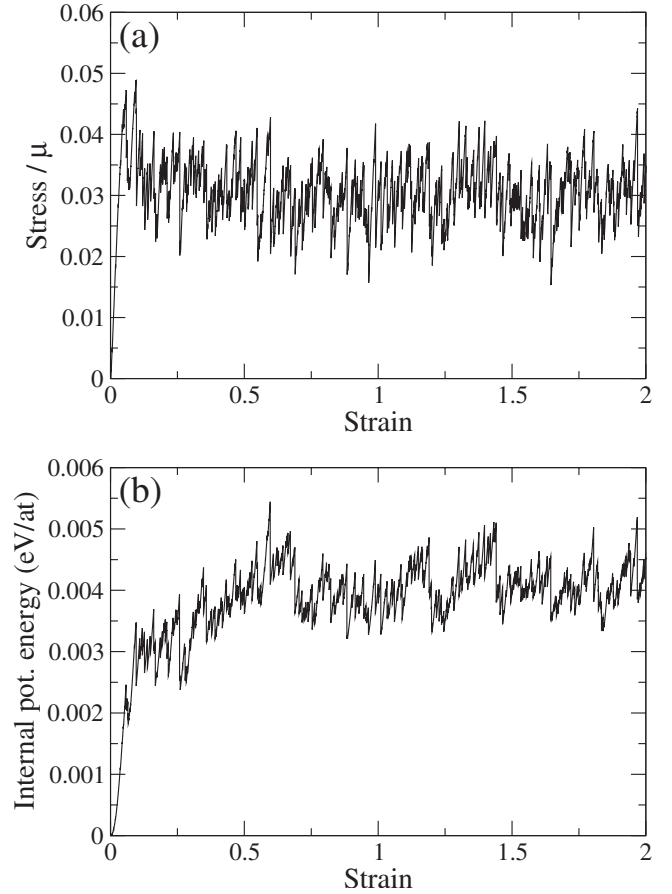


FIG. 2. Evolution of the average internal (a) shear stress and (b) potential energy during strain-controlled quasistatic shear deformation.

The stress-strain curve is composed of a linear elastic regime followed by a plastic regime that starts at an upper-yield point, which is evidence that the initial quenched configuration is well-relaxed.^{13,26} After about 50% strain, the glass enters a steady flow state where the shear stress fluctuates around a constant value, the flow stress, equal to about 0.03μ . As shown in Fig. 2(b), the internal potential energy also stabilizes around a well-defined average value of about 0.004 eV/atom.

In order to determine the yield stress with precision, stress-controlled simulations would be desirable. However, stress control is not generally possible using a quasistatic algorithm (i.e., small stress increments followed by energy minimizations) because such simulations are unstable: in the plastic regime, which starts at a stress close to the upper-yield point in strain-controlled deformation (0.046μ), the glass deforms continuously without finding another equilibrium configuration. This is a consequence of the lack of strain hardening in glasses deformed in simple shear, and a corollary of the existence of a steady state for this deformation geometry.

In the present article, we propose an alternative method whereby the deformation is effected through a Monte Carlo algorithm that allows for stress-controlled boundary conditions. The method is presented in Sec. II D and uses ART, described in Sec. II C, to find the elementary transitions. In

the remainder of this Section, we detail the algorithm used to minimize the potential energy of the glass at constant applied shear stress, a procedure required by ART.

The applied shear stress, τ_A , is controlled by using an equation of motion for the shift Δx with associated force $-L_X \cdot (\tau - \tau_A)$, where $\tau \equiv \sigma_{XY}$ is the average internal shear stress. The total potential energy of the glass, E_p , is then related to the internal potential energy E_I (energy of interatomic interactions) by the work of the applied stress:

$$E_p = E_I - \tau_A \cdot L_X \cdot \Delta x. \quad (1)$$

The total potential energy is minimized using a quenched dynamics algorithm, in which the motion of the atoms and evolution of the shift are treated separately. For the atoms, Newton's equations of motion are integrated accounting for inertia unless the scalar product of the 2N atomic velocity vector \mathbf{V} and the 2N force vector \mathbf{F} is negative, in which case \mathbf{V} is set to zero. Although this static algorithm is based on Newton's equations, it does not implement a true dynamics and the atomic masses and time step should be viewed as numerical parameters. Here, all atoms are assigned the same numerical mass and the integration parameter is $h \equiv dt^2/m = 0.04 \text{ \AA}^2/\text{N}$ with dt the numerical time step. Convergence is reached when the norm of the atomic force vector ($\|\mathbf{F}\|$, taken as the largest component of the vector in absolute value) is less than $F_C = 10^{-4} \text{ eV/\AA}$. In analogy with the FIRE algorithm,⁵³ convergence is accelerated by multiplying h by 1.2 at each time step when $\mathbf{V} \cdot \mathbf{F}$ has been positive for a minimum of 5 time steps, with a maximum integration parameter of four times its initial value. Quenched dynamics is also applied to Δx with an integration parameter $H = h/1000$ but the rate of change of Δx is reset to zero independently of atomic velocities and H is not rescaled during the minimizations.

C. Activation-relaxation technique

ART is an eigenvector-following method that allows sampling of the saddle points on a potential energy surface, connected to an initial equilibrium configuration. Saddle points, or activated states, have zero force ($\|\mathbf{F}\| < F_C$) and a Hessian matrix with exactly one negative eigenvalue. ART only requires computation of the lowest eigenvalue and associated eigenvector of the Hessian matrix, which are determined using the Lanczos algorithm,⁵⁴ an iterative method based only on force evaluations. Its convergence to the saddle was recently improved by Cancès *et al.*⁵⁵

Saddle points are found here at constant applied strain ($\Delta x = \text{constant}$) because the thermally activated escape to a saddle point is a rapid process that does not allow for stress relaxation. On the other hand, the relaxation from the activated to the final state is stress-controlled (same applied stress as the initial configuration) because the system is assumed to spend a sufficiently long time in the final state to allow for stress relaxations.

ART is an iterative method. We use the subscript n for all quantities computed at the n th step: \mathbf{x}_n the 2N vector of atomic configuration, \mathbf{F}_n , the force vector, C_n , the minimum eigenvalue, and \mathbf{T}_n the corresponding eigenvector. The cal-

ulation starts from an initial configuration, \mathbf{x}_0 , equilibrated under an applied stress τ_A . An initial direction in phase space, \mathbf{T}_0 , is chosen at random. In order to account for the localized nature of thermal activation, this vector contains only the random displacement of an atom chosen at random in the simulation cell. ART is then composed of three stages. In the first stage, the destabilization phase, the system is moved away from the basin of attraction of \mathbf{x}_0 along \mathbf{T}_0 using a step of fixed length, α^0 :

$$\mathbf{x}'_{n+1} = \mathbf{x}_n + \alpha^0 \mathbf{T}_0. \quad (2)$$

The configuration \mathbf{x}'_{n+1} is then relaxed perpendicularly to \mathbf{T}_0 using quenched dynamics. The relaxation is performed at constant applied strain which allows a strict perpendicularity with \mathbf{T}_0 to be maintained. The relaxation is limited to N_R^0 steps and leads to the configuration \mathbf{x}_{n+1} . The minimum eigenvalue of the Hessian matrix C_{n+1} and corresponding eigenvector \mathbf{T}_{n+1} are then computed approximately using the Lanczos algorithm with N_L iterations, starting from \mathbf{T}_n .

The above procedure is repeated until the minimum curvature becomes less than a critical negative value: $C_{n+1} < -C$ with $C > 0$. The algorithm then enters its second phase, the convergence phase, during which the system is brought to a saddle point by following the negative eigenvalue direction. The direction of motion is set to \mathbf{T}_n and the system is moved using a variable step length proposed in Ref. 55 and also included in the hybrid eigenvector-following method:⁴¹

$$\alpha'_n = \frac{\mathbf{T}_n \cdot \mathbf{F}_n}{C_n}. \quad (3)$$

If C_n is small in absolute value, α'_n may diverge and a cutoff has to be used. Different solutions have been proposed.^{41,55} Here, we simply limit the step length to a maximum value: $\alpha_n = \min(\alpha'_n, \alpha^1)$. The system is then displaced according to:

$$\mathbf{x}'_{n+1} = \mathbf{x}_n + \alpha_n \mathbf{T}_n \quad (4)$$

and relaxed perpendicularly to \mathbf{T}_n within a maximum number of steps N_R^1 . Convergence near the saddle is accelerated by incrementing N_R^1 by 1 each time $\alpha'_n < \alpha^1$. C_{n+1} and \mathbf{T}_{n+1} are then computed using the Lanczos algorithm, starting from \mathbf{T}_n with N_L steps. \mathbf{T}_{n+1} is oriented such that $\mathbf{T}_{n+1} \cdot \mathbf{F}_{n+1} < 0$, in order to move the system away from the initial configuration.

This procedure is iterated until either convergence (i.e., $\|\mathbf{F}_n\| < F_C$) or C_n becomes positive again. The latter usually means that the system has fallen back into the basin of attraction of \mathbf{x}_0 : the search is then deemed unsuccessful and another search is started.

Once a saddle point is found, its activation energy is given by the difference in internal potential energy between initial and activated states. ART then enters its third phase, the relaxation phase. The system is perturbed along \mathbf{T}_n toward \mathbf{x}_0 and relaxed at constant applied strain using quenched dynamics to check that the saddle point is connected with \mathbf{x}_0 . If not, the saddle point is deemed nonconnected; it is rejected and a new search is started. If the saddle is connected, the system is perturbed along \mathbf{T}_n away from \mathbf{x}_0 and relaxed at

TABLE I. Parameters used in ART. α^0 and α^1 are given in \AA and C in $\text{eV}/\text{\AA}^2$.

α^0	N_R^0	N_L	C	α^1	N_R^1
0.1	5	10	0.01	0.5	5

constant applied stress τ_A , in order to determine the final configuration. The inelastic strain γ_I associated with the transition is then given by:

$$\gamma_I = \frac{\Delta x_F - \Delta x_I}{L_Y} \quad (5)$$

where $\Delta x_F - \Delta x_I$ is the difference in shift between initial and final configurations.

In the present work, ART involves the numerical parameters listed in Table I. They must be optimized carefully because they strongly influence the efficiency of the method, which depends on various factors. The first such factor is the average number of force evaluations per saddle point. Second is the fraction of unsuccessful searches, which is the fraction of searches where C_n becomes positive during a convergence phase. Third is the fraction of nonconnected saddles, where the search leads to a saddle not connected with the initial configuration. Lastly is the bias toward low-energy barriers: ART is known to be biased toward low-energy barriers^{45,56} and some parametrizations make the bias even stronger. The number of Lanczos iterations, N_L , should always be kept low to minimize the number of force calls. α_0 , N_R^0 , and C control the energy and degree of relaxation of the system at the end of the destabilization phase, which strongly impact the convergence phase. α_0 and N_R^0 control the relaxation perpendicular to \mathbf{T}_0 . If α_0 is too small or N_R^0 too large, the system tends to remain at the bottom of the attraction basin, lengthening the destabilization phase and favoring low-energy barriers. On the other hand, if α_0 is too large or N_R^0 too small, the system is taken very far from equilibrium, which increases the fraction of nonconnected saddles. A small C shortens the destabilization phase and avoids taking the system too far from \mathbf{x}_0 , thus decreasing the fraction of nonconnected saddles, but it also increases the risk of relaxation back into the initial basin during the first steps of the convergence phase, thus increasing the fraction of unsuccessful searches. On the other hand, a large C increases the fraction of nonconnected saddles. α^1 and N_R^1 control the convergence phase and are the most important parameters. They must be optimized together in order to be correctly balanced. The difficulty comes from the fact that at the end of the destabilization phase, the glass is of high energy, higher than the saddle energy in most cases, and of high internal force $\|\mathbf{F}_n\|$. During the first steps of the convergence phase, the system has to be brought closer to the saddle, which is controlled by α^1 because at the beginning of the convergence the step length obtained from Eq. (3) is large and usually exceeds α^1 . And the relaxation perpendicular to \mathbf{T}_n , controlled by N_R^1 , must not be too fast otherwise the glass returns to the initial basin of attraction. It must not be too slow, either, or the glass energy and force keep increasing

and the calculation does not converge. Closer to the saddle, when the step length in Eq. (3) becomes less than α^1 , the relaxation perpendicular to \mathbf{T}_n should be better in order to accelerate the convergence to the saddle. For this reason, in the present algorithm, N_R^1 is incremented near the convergence.

These numerical parameters are also strongly system dependent. They can be optimized for a given microstructure, but it is difficult to find a set of parameters efficient for all microstructures, for instance before and after deformation where the glass contains very different fractions of low-energy barriers, as will be seen in the following. The values given in Table I represent a compromise that allows calculations on all of the various types of microstructures considered here. Also, we determine usually 4000 saddles per configuration and as the size of the sample grows, the number of redundant saddles (saddles already determined) increases. These saddles are also rejected, which further decreases the efficiency of the calculations. On average, in order to determine 4000 saddles in a well-relaxed glass, 30000 searches are needed (including successful and unsuccessful searches as well as nonconnected and redundant saddles) for a total number of force evaluations of about 15×10^6 .

As a reference, Fig. 3 shows the distributions of activation energies and inelastic strains in the initial quenched glass. Distributions are shown for samples of different sizes, containing from 500 to 4000 saddle points. These numbers are small compared to the total number of saddles estimated in Ref. 56 for amorphous silicon, given as 30 to 60 times the number of atoms. However, we can see in Fig. 3 that they are sufficient to capture the shape of the distributions. Figure 3(a) illustrates the bias of ART toward low-energy barriers: as the sample size increases, the fraction of energy barriers below the maximum of the distribution decreases while the fraction of barriers above the maximum increases. Correspondingly, the average activation energy, calculated from the distributions and given in the legend of Fig. 3, increases with the sample size. No bias is visible in the distributions of inelastic strains shown in Fig. 3(b), which are all peaked at zero strain with negligible average values. In the following, all distributions were obtained from samples containing 4000 events in order to yield the best description of the potential energy surface.

D. Monte Carlo algorithm

The metallic glass is deformed here at constant applied stress using a Monte Carlo method. The following procedure is iterated at each step, starting from an equilibrium initial configuration. First, ART is used to find a transition from the current state. Since the initial direction of motion, \mathbf{T}_0 , is chosen at random, the activated state can be considered as randomly selected from among all possible transitions. After relaxation away from the saddle, the difference in total potential energy between initial and final states ΔE_p is computed. If $\Delta E_p < 0$, the transition is accepted and the final state is taken as the current configuration. If $\Delta E_p > 0$, the transition is rejected, the current configuration is maintained and ART is called again from that configuration.

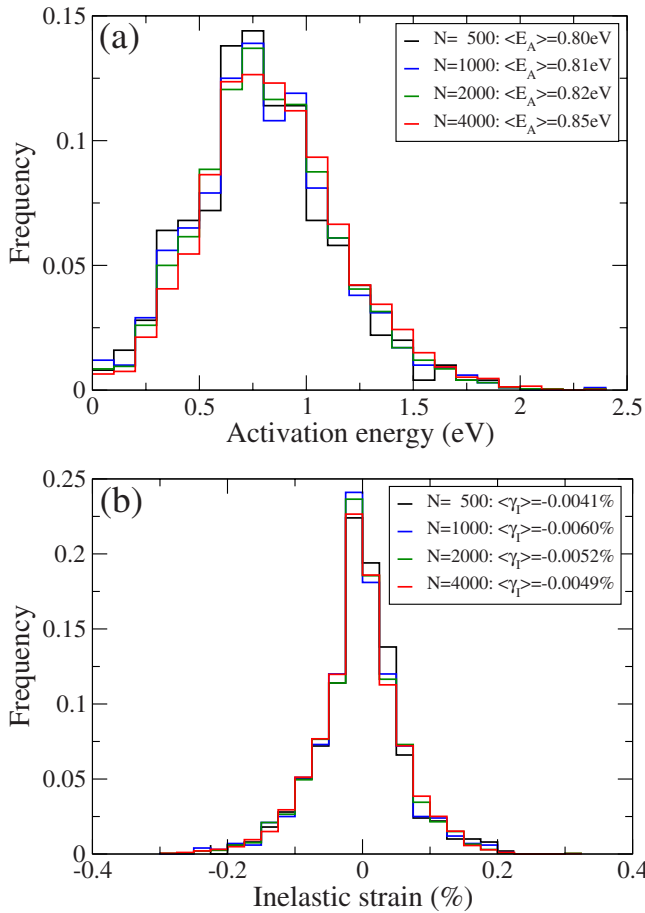


FIG. 3. (Color online) Distributions of (a) activation energies and (b) inelastic strains in a glass quenched from 2000 K at 10^{11} K.s $^{-1}$. The distributions were obtained from samples containing different numbers of saddle points noted in the legend of the figure, along with the distribution averages. The bin size for activation energies is 0.1 eV, and for strains 0.025%.

The algorithm is iterated until either a maximum strain level (set to 600%) is achieved or a maximum number of rejected transitions (set to 600) are reached. The latter case thus occurs when 600 transitions are found from a given configuration that all lead to final configurations with higher total potential energies than the current configuration. We then judge that the glass has reached its ground state, which is called a jammed state. In the former case, the glass accumulates deformation and we will see in the following that it reaches a steady state that we will refer to as a flow state.

III. SIMULATION RESULTS

A. Jamming-unjamming transition

We performed Monte Carlo simulations for a range of applied stresses below the stress-controlled elastic limit (0.046μ). The initial configurations were obtained from the quenched glass by increasing the applied stress quasistatically up to the desired stress. Figure 4 shows the evolution of the total and internal potential energies of the glass as a function of accumulated inelastic strain during simulations at

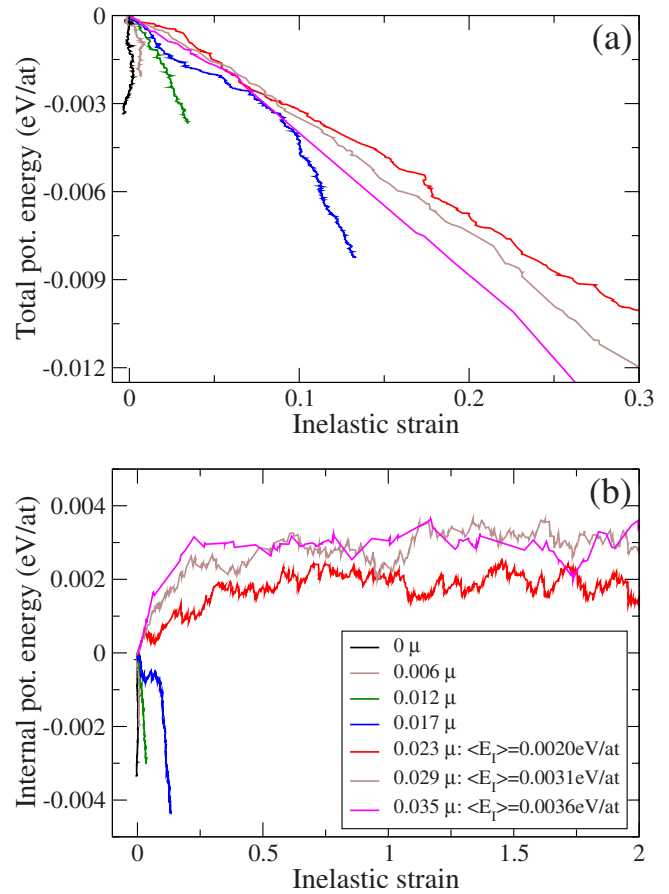


FIG. 4. (Color online) Evolution of the (a) total and (b) internal potential energies as a function of accumulated inelastic strain during Monte Carlo simulations at different applied stresses noted in the legend of the figure. Deformations up to six were simulated but for the sake of clarity, strains in (a) are limited to 0.3 and in (b) to 2. The reference energies and strains are those of the initial configuration (initial quenched glass relaxed under the desired applied stress). The average internal potential energies in the flowing regime are given in the legend of the figure.

different applied stresses. When no stress is applied (black curve), the internal potential energy (equal to the total potential energy in this case since $\tau_A=0$, see Eq. (1)) decreases throughout the simulation, which stopped after 545 Monte Carlo steps when the glass reached a jammed state. This process corresponds to aging of the glass toward a low-energy configuration.

The same behavior is obtained for applied stresses up to $\tau_A=0.017 \mu$: the glass accumulates some strain, but the latter remains small ($<15\%$) and the glass converges to a jammed state. The situation is different at $\tau_A=0.023 \mu$, where the glass reaches a flow state: it does not converge to a state of minimum total potential energy but accumulates up to 600% deformation, at which point the simulation is stopped. Unbounded flow was obtained at all stresses above $\tau_A=0.023 \mu$. We note that in this regime, flow remains homogeneous and no persistent shear band forms.

The simulations thus evidence a jamming-unjamming transition^{6,57} between aging and shear flow at a critical applied stress, which defines the yield stress of the glass. The

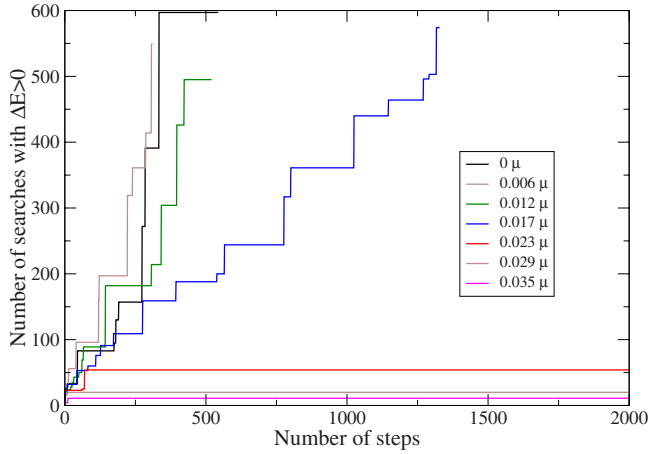


FIG. 5. (Color online) Evolution of the maximum number of searches per Monte Carlo step during simulations at different applied stresses noted in the figure.

latter was found here equal to $0.022 \pm 0.002 \mu$. We tested its dependence on the direction of shear and found the same yield stress in both positive and negative X directions as well as in positive and negative Y directions (obtained by rotating the simulation cell).

The jamming-unjamming transition is clearly visible in Fig. 4(b), which shows the internal potential energy of the glass. By construction of the method, the total potential energy decreases at each Monte Carlo step but the internal potential energy (which does not account for the work of the applied stress, see Eq. (1)) may increase or decrease. Figure 4(b) shows that below the yield stress, the internal potential energy decreases from the beginning of the simulations while above the yield stress, it initially increases and after about 50% strain reaches a steady-state value that increases with the applied stress.

The transition also appears in Fig. 5, which reports the evolution of the maximum number of rejected transitions per step since the beginning of simulations, at different applied stresses. Above the yield stress, the maximum number of rejected transitions is small, less than 50; this indicates that in a yielding glass, there are many saddle points that lead to lower-energy configurations. In contrast, in the jamming regime, the maximum number of rejected transitions increases roughly linearly with the number of steps, meaning that the states of decreasing internal potential energy visited by the glass during aging are surrounded by an increasing fraction of higher-energy states.

B. Recovery

We tested the dependence of the flow limit on the initial state of the glass by performing recovery simulations below the yield stress, starting from configurations obtained above the yield stress. More specifically, we generated initial configurations from the last configuration obtained in the flowing regime at $\tau_A = 0.023 \mu$ and relaxed at various stresses below the elastic limit. Figure 6 shows the resulting evolutions of total and internal potential energies. For comparison, the figure also shows the evolution if the applied stress is

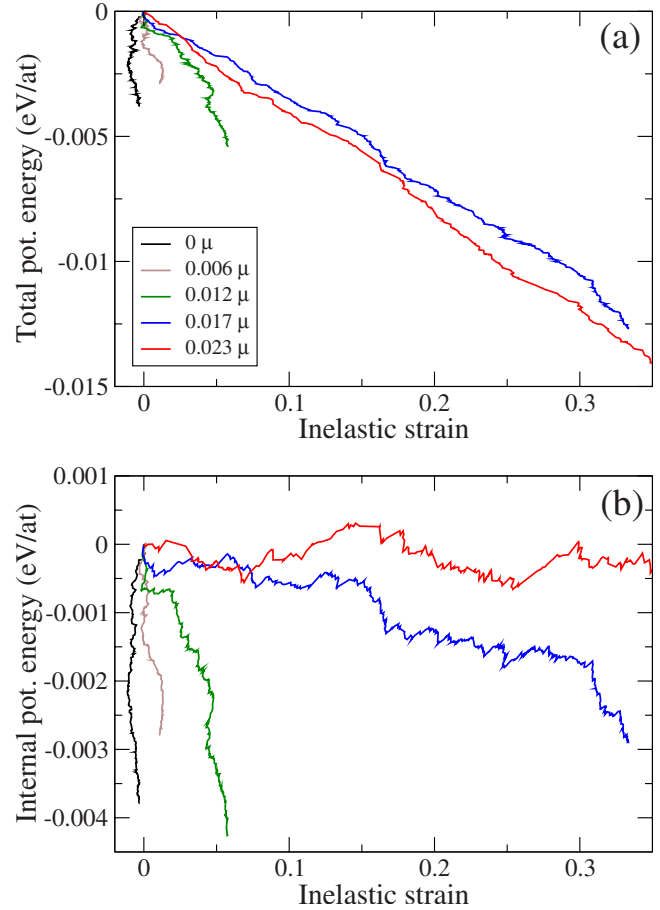


FIG. 6. (Color online) Evolution of the total (a) and internal (b) potential energies as a function of accumulated strain during Monte Carlo simulations at different applied stresses noted in the figure. The initial configurations were obtained by relaxing at the desired stresses the final configuration obtained in the flow state at 0.023μ (red curve in Fig. 4). The reference energies and strains are those of the initial configurations.

maintained at $\tau_A = 0.023 \mu$. Below the yield stress, the internal potential energy decreases during the simulations and even though at 0.017μ a substantial deformation is produced (35%), the glass systematically relaxes to a jammed state, while at 0.023μ , the glass flows without limit. This confirms that the jamming-unjamming transition is independent of the initial configuration.

C. Minimum energy state microstructures

One approach to characterize the microstructure of a 2D glass is to consider its Voronoi tessellation, as originally proposed by Deng *et al.*⁹ Figure 7 shows two extreme cases: sections of the jammed state obtained at 0μ and of the final configuration in the flow state at 0.035μ . The atoms are colored according to the number of sides of their Voronoi polygon. As reported in Ref. 9, the microstructures are composed of regions of quasiorder where the atoms have six-sided polygons and appear in yellow, separated by strings of atoms having five- and seven-sided polygons that appear in blue in Fig. 7. Comparison of the two microstructures shows

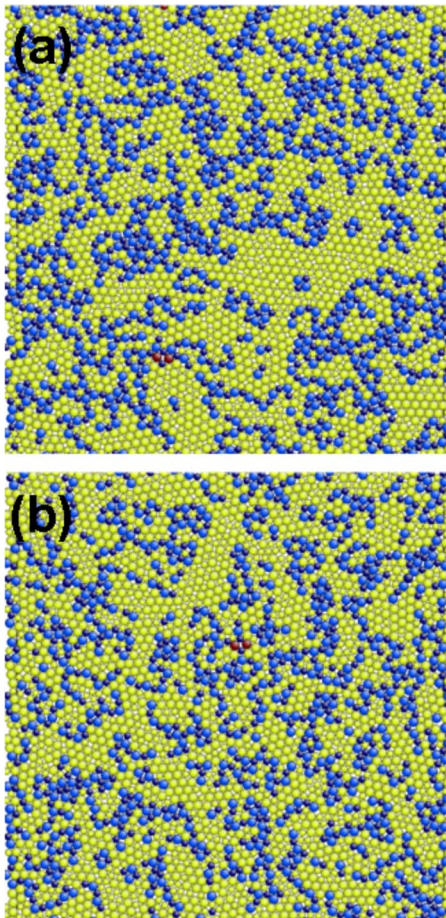


FIG. 7. (Color online) Atomic configurations in (a) the jammed state obtained at 0μ and (b) the flow state at 0.035μ . The color of the atoms depends on the numbers of sides of their associated Voronoi polygon: yellow for 6 sides, dark blue for 5, and light blue for 7. The same section of the simulation cell is shown in both figures.

that aging did not induce a crystallization of the glass and that shear flow did not significantly change the microstructure: the size of the quasiordered regions is somewhat smaller after deformation but the region of five- and seven-sided polygons are thinner, such that their density is the same in both microstructures.

The effect of shear flow is more clearly identified by considering the distributions of activation energies and inelastic strains as determined by ART. In Ref. 46 we reported such distributions for the case of quasistatic deformation; in Fig. 8 we show them for various minimum-energy states. The initial configurations are the final states obtained at the different applied stresses, quasistatically unloaded down to zero internal average shear stress. This unloading is effected to remove the stress bias we reported in Ref. 46: most events under stress are in the direction of the stress, so information specific to the microstructure is best revealed when the average internal stress is zero. The stresses noted in Fig. 8 thus do not refer to the actual internal average shear stress in the glass (which is systematically less than $3 \times 10^{-5} \mu$), but to the stresses applied during the initial phase of deformation. In order to be consistent with the Monte Carlo simulations, ac-

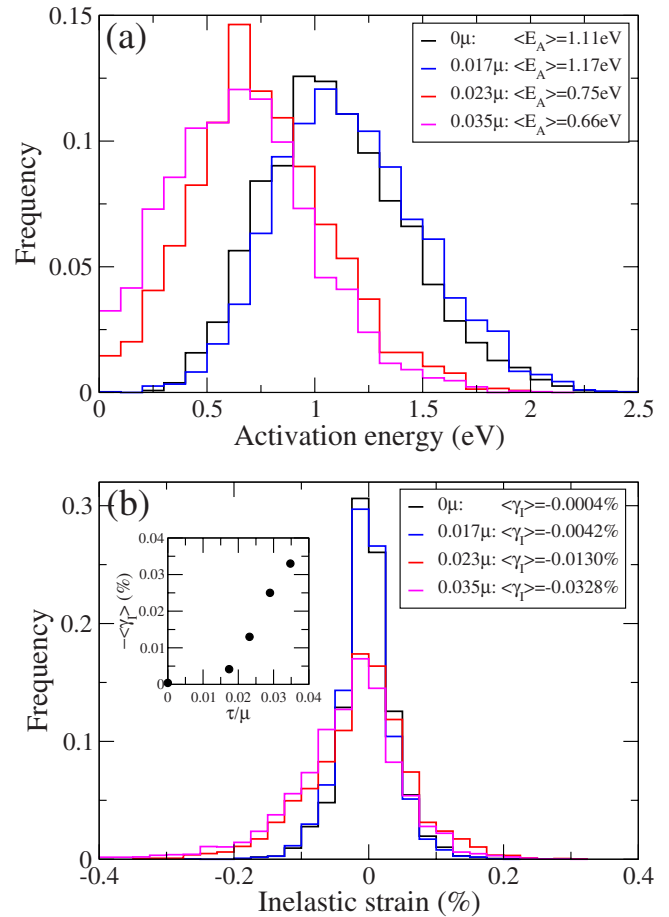


FIG. 8. (Color online) Distributions of (a) activation energies and (b) inelastic strains in the microstructure of minimum-energy states obtained by Monte Carlo simulations at different stresses noted in the figure along with the distribution averages. All configurations were elastically unloaded down to zero average internal shear stress before their energy landscape was sampled.

tivated states are obtained at constant applied strain while relaxation to the final state is stress controlled with zero applied stress.

We consider first the distributions of activation energies shown in Fig. 8(a). Below the yield stress ($\tau_A < 0.022 \mu$), the distributions contain no activation energies below 0.25 eV. By comparison, the distribution in the initial quenched glass (Fig. 3(a)) contains more low-energy barriers: 1% of them are below 0.1 eV. The jammed state reached during aging is therefore of higher stability in the sense that it is separated from other states by higher-energy barriers. By contrast, above the yield stress ($\tau_A > 0.022 \mu$), the distributions contain a high density of low-energy barriers, the density of which increases with applied stress. The flow state reached during deformation is therefore of both higher internal potential energy and lower stability. Creation of low-energy barriers was also observed after quasistatic strain-controlled plastic deformation⁴⁶ with a fraction of barriers below 0.1 eV close to 9%, much higher than in the present case.

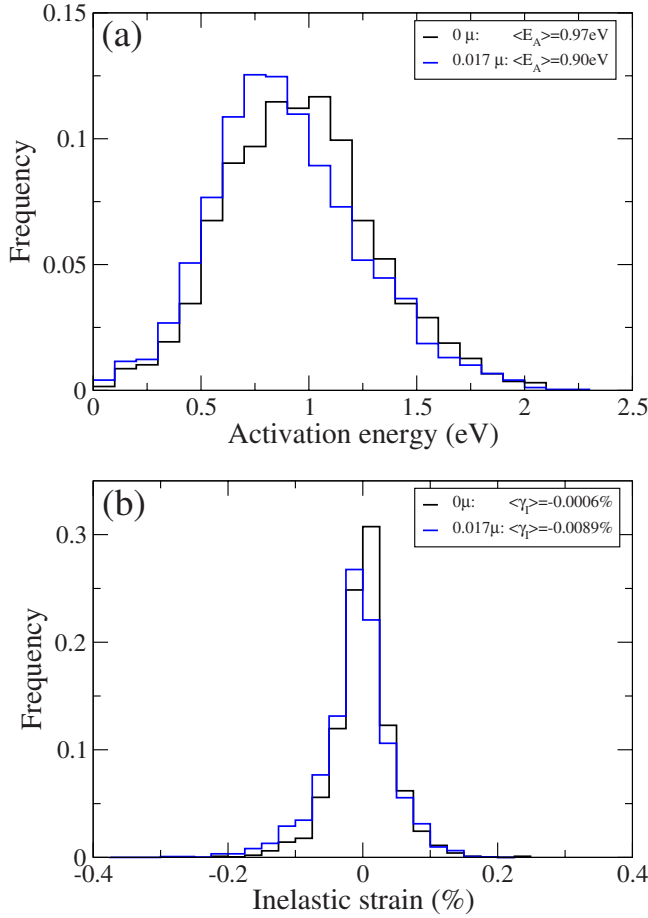


FIG. 9. (Color online) Distributions of (a) activation energies and (b) inelastic strains in jammed states obtained at 0 and 0.017μ after the recovery shown in Fig. 6 and elastic unloading.

The effect of deformation is visible in the distributions of inelastic strains shown in Fig. 8(b). In all cases, the distributions are peaked at zero strain because of the zero internal average shear stress, but below the yield stress, the distributions are symmetrical with a small range, while above the yield stress they are asymmetrical with a long tail in the negative strain region. This asymmetry is characteristic of the flowing regime, as shown by the inset in Fig. 8(b) where we see that the average strain starts to deviate significantly from zero only at the yield stress. The same effect was found previously in quasistatically strained samples.⁴⁶ This asymmetry reflects the polarization of the microstructure acquired by the glass during shear deformation, which is a consequence of the strong influence of the history of deformation on these systems. This point is further discussed in Sec IV D.

A high density of low-energy barriers and a nonzero average inelastic strain are the two main characteristics of the flow state. This conclusion is confirmed in Fig. 9, which shows the energy and strain distributions in two jammed states obtained after recovery as presented in Sec. III B. Comparison with the initial distributions (red curves in Fig. 8) shows that during recovery, the fraction of low-energy barriers decreases, as well as the average inelastic strain (in absolute value).

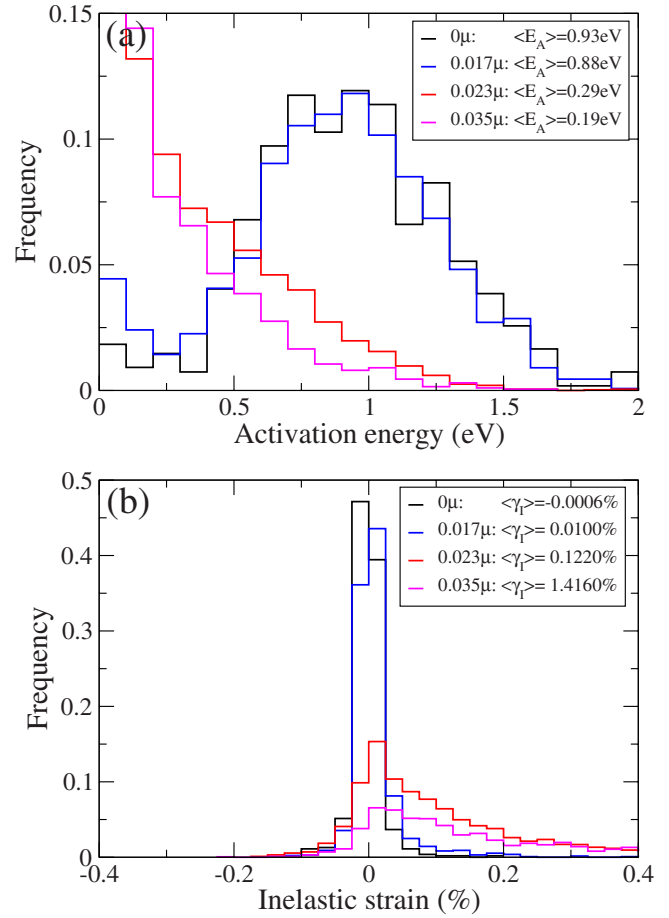


FIG. 10. (Color online) Distributions of (a) activation energies and (b) inelastic strains of the transitions accepted during Monte Carlo simulations at different applied stresses noted in the figure. The distributions are computed from the same simulations as shown in Fig. 4.

D. Distributions during Monte Carlo simulations

Figure 10 shows the distributions of activation energies and inelastic strains computed from the elementary transitions accepted during Monte Carlo simulations at different applied stresses. This figure makes apparent the marked difference between the states below and above the yield stress. In the flowing regime, the maximum of the energy distribution is at zero energy and the distribution of inelastic strains is strongly shifted toward positive strain events, which is partly due to the stress-bias induced by the applied shear stress. On the other hand, during aging, the distribution of activation energies resembles that of the activation energies in the microstructure shown in Fig. 8 and the strain distribution is peaked at zero. We note however that the energy distributions in Fig. 10 contain more low-energy barriers than those in Fig. 8. This is due to the bias of ART toward low-energy barriers, which have a larger statistical weight in the distribution of first accepted transitions than in the full distribution of transitions for a given configuration.

The thermally activated events that constitute these distributions are similar to those observed in quasistatic shear deformation. Events with small associated inelastic strain (typi-

cally below 0.10% strain) are localized, while larger strain events form avalanches that span across the entire simulation cell. In this relatively high-density glass, we do not see diffusionlike events. All events, even in the absence of applied stress, induce a shear of the structure.

IV. DISCUSSION

A. Comparison between Monte Carlo and quasistatic simulations

We propose here a Monte Carlo approach to simulate aging and shear flow in glasses. Checking the connectivity between initial, activated, and final states found by ART ensures that the transitions undergone by the glass are physical processes representative of dynamical simulations. The present method can be distinguished from quasistatic simulations in two main aspects. First, it is stress control that allows the simulation of a wide range of applied stresses and precise determination of the yield stress. By contrast, in quasistatic simulations, the glass is mechanically forced to deform by application of increasing strains and the stress cannot be controlled, but arises from the dependence of the internal potential energy on strain.¹⁵ The second advantage is that the present simulations are not limited by thermal activation. They enable us to investigate the long-time behavior of the glass at low temperature and to ask whether it converges to a state of minimum energy or finds a steady flow state. In quasistatic simulations, only strain-induced transitions are possible, which forbids the thermal relaxations that give rise to aging.

We note that nevertheless, the elementary inelastic events that occur during Monte Carlo simulations closely resemble those observed in quasistatic simulations: the small strain events we find with this method are in fact localized shear zones as proposed by Argon,⁵⁸ while the larger strain events proceed by avalanches of rearrangements that span the entire simulation cell.^{14,17,20} Also, in both Monte Carlo and quasistatic simulations, the steady state is reached after about 50% strain, as shown in Figs. 2 and 4.

In terms of computing power, the number of force calls per Monte Carlo step depends strongly on the number of rejected transitions. The simulation cost increases near the jamming-unjamming transition, in particular below the yield stress, where the relaxation to a jammed state is gradual and involves many rejected transitions toward the end of the simulation. Quantitatively, the total number of force calls required to reach 200% strain at 0.035μ (well-above the transition) is 1.65×10^6 , including those used in exploring unsuccessful and nonconnected saddles. It increases up to 34×10^6 at 0.023μ (close to the transition). An equivalent quasistatic simulation with strain increments of 10^{-4} and full relaxations between increments requires about 2.5×10^6 force calls. Above the transition, the present method is thus faster than a quasistatic simulation because stress-controlled elementary events can produce large strains, while close to the transition, it is slower. Also, in the latter case the yield stress can be determined from much shorter simulations thanks to the marked evolutions of the inelastic strain, inter-

nal potential energy and number of rejected transitions at the yield stress, as shown in Figs. 4 and 5.

B. Stress-induced jamming-unjamming transition

The Monte Carlo simulations evidence a transition between aging to a jammed state (at low applied stresses) and shear flow into a steady flow state (at high stresses). The transition is sharp and clearly visible in the evolutions of inelastic strain [Fig. 4(a)], internal potential energy [Fig. 4(b)] and rejected transitions (Fig. 5). We also showed that it is independent of the initial configuration of the glass (Fig. 6). This transition corresponds to the stress-induced jamming-unjamming transition first discussed in the context of granular materials^{3,57} and studied experimentally in such materials^{59,60} and in colloidal pastes^{61,62} among others.

The transition is shown here to occur for an applied shear stress equal to $\tau_A = 0.022 \pm 0.002 \mu$. This stress is well defined, since just below it the internal potential energy of the glass decreases rapidly in the simulations and the numbers of rejected transitions increases, while just above the opposite evolutions are observed. Interestingly, the yield stress found here is significantly lower than the threshold stresses obtained with quasistatic strain-controlled simulations shown in Fig. 2, both the upper-yield point ($\sim 0.046 \mu$, which is also the elastic limit with stress-controlled boundary conditions) and the steady-state flow stress ($\sim 0.03 \mu$). This is reflective of the fact that quasistatic simulations do not give access to the long-time behavior of the glasses because they do not account for thermal activation. As stated above, the same is true for finite-temperature simulations based on molecular dynamics. The yield stresses extrapolated from athermal stress-controlled simulations in a granular medium in Ref. 63, as well as those extrapolated from finite-temperature strain-rate controlled simulations in a Lennard-Jones glass in Refs. 21 and 22 are thus likely overestimated.

C. Relaxation- vs stress-driven events

We have seen in Fig. 4(b) that the internal potential energy of the glass decreases during aging whereas in the flowing regime, it first increases and then saturates in steady state. The internal potential energy may increase or decrease because it does not account for the work of the applied stress (Eq. (1)). The latter introduces a tilt to the potential energy surface in the direction of positive strain, which may change the sign of the total potential energy difference between initial and final states. The final state may thus be of higher internal potential energy (i.e., energy in absence of applied stress) but of lower total potential energy (i.e., energy under stress) if the transition produces a sufficiently large strain. We note that an increase in internal potential energy physically means introduction of damage into the glass microstructure; this however is difficult to identify in the microstructure itself, as illustrated in Fig. 7. The glass is in a state of compression after shear deformation, implying a production of free volume but the latter remains small and does not lead to the formation of voids, for example.

One should therefore distinguish two types of thermally activated transitions in glasses. The first type are those tran-

sitions that lead to a state of lower internal potential energy, i.e., which are energetically favorable even in the absence of applied stress. We call these *relaxation-driven transitions* because, as we will see in the following, they lead to states that are more stable both dynamically and thermodynamically. The second types are those transitions that lead to states of higher internal potential energy but lower total potential energy. We call these *stress-driven transitions* because they are not energetically favorable in the absence of applied stress, and therefore are the events that accumulate damage in the glass structure.

With these two types of transitions defined, we propose that the yield stress corresponds to the minimum applied stress that sufficiently tilts the potential energy surface to allow for stress-driven transitions. Indeed, Fig. 4(b) shows that below the yield stress, the great majority of transitions are relaxation driven and both the internal and total potential energies decrease during the simulation. The applied stress is thus not strong enough to significantly alter the respective stability of inherent structures. On the other hand, above the yield stress, the first transitions are mostly stress driven and increase the internal potential energy of the glass. As the internal potential energy increases, the probability of finding a relaxation-driven transition increases and the steady state is reached when an equilibrium between relaxation-driven and stress-driven transitions is achieved.

We see from Fig. 4(b) that in the flowing regime, the steady state average internal potential energy is an increasing function of the applied stress, which reaches 0.0036 eV/atom at 0.035μ . In quasistatic simulations (Fig. 2), the steady state average internal potential energy is higher (0.004 eV/atom), consistent with the fact that bringing the glass to positions of instability before each plastic transition favors higher-energy microstructures.

Since the internal potential energy decreases during aging, the jammed states are thermodynamically more stable than the initial quenched glass. They are also more stable dynamically because, as shown in Fig. 8(a), they are surrounded by higher activation energy barriers. Quantitatively, the jammed states have no barrier below 0.25 eV while the initial quenched glass has a small but significant fraction of barriers of about 0.6% below 0.1 eV. We tested the stability of the jammed state obtained at $\tau_A=0 \mu$ by performing a molecular dynamics simulation involving annealing at 300 K for 0.5 ns: after an energy minimization, the glass returned to its initial configuration. On the other hand, the flow states reached above the yield stress are only marginally stable since, as shown in Fig. 8(a), they contain a significant fraction of energy barriers below 0.1 eV; this leads to a rapid evolution of the glass microstructure in a dynamical simulation. This point was checked by performing molecular dynamics simulations at 300 K as above, with the result that the glass had transitioned to a new inherent structure after only 0.4 ps.

Our calculations thus evidence a strong relation between the internal potential energy of a state and its stability: the lower the internal potential energy, the higher its surrounding activation energies (i.e., the deeper its basin of attraction). This scaling appears to be a general property of potential energy landscapes, as discussed by Debenedetti and Stillinger.⁶⁴

D. Polarization

The glass microstructure after shear flow is specific and characteristic of the flow leading to it, because of its polarization. Deformation-induced polarization was first discussed by Argon and Kuo,³¹ and was also reported in our previous study on the quasistatic deformation of the present simulated system.⁴⁶ Polarization is evidenced here by the asymmetry of the inelastic strain distributions in the flowing regime [Fig. 8(b)]. Physically, polarization arises because in the initial phase of deformation, the glass accumulates positive strain events that leave a signature in the glass microstructure. Escaping from this configuration is therefore more likely to involve a negative strain event that removes some of the excess positive strain, implying an asymmetrical inelastic strain distribution. We note that polarization depends on the symmetry of the strain tensor. Simple shear is certainly the most favorable state to induce polarization, while we expect that isotropic deformation (compression or expansion) would not induce any shear anisotropy.

We find that polarization cannot be easily detected in the present glass microstructure. In particular, it does not come from a simple anisotropy of nearest-neighbor bonds. This contrasts with amorphous silicon where anisotropic distributions of atomic bonds have recently been evidenced after plastic strain, using the fabric tensor.⁶⁵ We computed the fabric tensor on the present structures in the jammed and flowing regimes but found no significant evolution. The reason is presumably the absence of angular terms in the interatomic potentials used here.

Polarization leads to strain recovery during aging of deformed microstructures, as evidenced by the negative macroscopic strain during aging with no applied stress in Fig. 6. Strain recovery was used by Argon and Kuo³¹ to determine the distribution of thermally activated events in a metallic glass, and was also observed experimentally in colloidal pastes.⁶² It originates from the removal of the polarization of the initial state that involves an excess of negative strain events. Strain recovery is however small in the present system and is masked when a positive stress is applied, as seen in Fig. 6.

It has been argued in the literature that temperature and applied stress play similar roles in jamming systems,⁵⁷ a concept supported by the existence of an effective temperature that describes driven athermal disordered systems, as shown numerically in a number of atomic systems.^{22,23,30} Indeed, shear flow in the present simulations brings the glass to a high-energy state, with an energy that increases with applied stress, as would be obtained by application of an elevated temperature. This process, which opposes aging, has been named rejuvenation in the simulation¹³ and experimental^{66,67} literature.

The present results, however, speak against the simple analogy between temperature and deformation. The phenomenon of polarization shows that an increase in temperature does not bring the glass to the same position in the potential energy landscape as does an applied stress, at least not in the case of a simple shear. An increase in temperature has a negligibly small probability to bring the glass to a polarized state; the effect of temperature is isotropic. Stress-driven pro-

cesses should therefore be distinguished from rejuvenation, as in the theory of shear band propagation of Shimizu *et al.*^{28,29} who proposed to call this process alienation.

Based on these considerations, we speculate that capturing the state of the glass in a single variable may not be possible. Instead, the effective temperature could perhaps be defined as a tensor in order to reflect the symmetry of the strain tensor. Similarly, the notion of “free volume” as a glass state variable may capture isotropic effects in a manner similar to the effective temperature, but cannot account for polarization. We note here a possible analogy with theories of crystalline anisotropic plasticity where damage is represented by a tensor.⁶⁸ These conjectures require considerable additional investigation. In any event, the present Monte Carlo approach to simulate glass flow at long times may provide a useful tool to explore the details of extrinsic driving forces and how they influence the energy landscape.

V. CONCLUSION

We have proposed here an alternative approach to conventional molecular statics and dynamics based on Monte

Carlo simulations in an off-lattice disordered system. Although the work presented here is restricted to two dimensions, its extension to three dimensions is straightforward. We have shown that accounting for thermal activation through the use of the activation-relaxation technique significantly reduces the yield stress compared to estimates based on quasistatic simulations. This method also gives access in a single framework to both aging and flow, and sampling the energy landscape has proved to be a useful method to characterize the microstructure of minimum-energy states, both below and above the yield stress.

ACKNOWLEDGMENTS

The authors would like to thank E. Homer for insightful discussions. This work was funded by the Délégation Générale à l’Armement. C.A.S. acknowledges support from the U.S. Office of Naval Research under Contract No. N00014-08-1-0312.

*On sabbatical leave from the Institut Polytechnique de Grenoble, France.

- ¹C. A. Schuh, T. C. Hufnagel, and U. Ramamurty, *Acta Mater.* **55**, 4067 (2007).
- ²P. Schall, D. Weitz, and F. Spaepen, *Science* **318**, 1895 (2007).
- ³M. E. Cates, J. P. Wittmer, J. P. Bouchaud, and P. Claudin, *Phys. Rev. Lett.* **81**, 1841 (1998).
- ⁴D. Rodney, M. Fivel, and R. Dendievel, *Phys. Rev. Lett.* **95**, 108004 (2005).
- ⁵P. Hébraud, F. Lequeux, J. P. Munch, and D. J. Pine, *Phys. Rev. Lett.* **78**, 4657 (1997).
- ⁶*Jamming and Rheology*, edited by A. J. Liu and S. R. Nagel (Taylor & Francis, New York, 2001).
- ⁷S. Kobayashi, K. Maeda, and S. Takeuchi, *Acta Mater.* **28**, 1641 (1980).
- ⁸D. Srolovitz, V. Vitek, and T. Egami, *Acta Mater.* **31**, 335 (1983).
- ⁹D. Deng, A. S. Argon, and S. Yip, *Philos. Trans. R. Soc. London, Ser. A* **329**, 549 (1989).
- ¹⁰D. L. Malandro and D. J. Lacks, *Phys. Rev. Lett.* **81**, 5576 (1998).
- ¹¹M. L. Falk and J. S. Langer, *Phys. Rev. E* **57**, 7192 (1998).
- ¹²D. L. Malandro and D. J. Lacks, *J. Chem. Phys.* **110**, 4593 (1999).
- ¹³M. Utz, P. G. Debenedetti, and F. H. Stillinger, *Phys. Rev. Lett.* **84**, 1471 (2000).
- ¹⁴C. E. Maloney and A. Lemaître, *Phys. Rev. Lett.* **93**, 016001 (2004).
- ¹⁵C. E. Maloney and A. Lemaître, *Phys. Rev. Lett.* **93**, 195501 (2004).
- ¹⁶M. J. Demkowicz and A. S. Argon, *Phys. Rev. Lett.* **93**, 025505 (2004).
- ¹⁷M. J. Demkowicz and A. S. Argon, *Phys. Rev. B* **72**, 245206 (2005).

- ¹⁸A. Tanguy, F. Leonforte, and J. L. Barrat, *Eur. Phys. J. E* **20**, 355 (2006).
- ¹⁹C. E. Maloney and A. Lemaître, *Phys. Rev. E* **74**, 016118 (2006).
- ²⁰N. P. Bailey, J. Schiotz, A. Lemaître, and K. W. Jacobsen, *Phys. Rev. Lett.* **98**, 095501 (2007).
- ²¹L. Berthier and J. L. Barrat, *J. Chem. Phys.* **116**, 6228 (2002).
- ²²L. Berthier and J. L. Barrat, *Phys. Rev. Lett.* **89**, 095702 (2002).
- ²³I. K. Ono, C. S. O’Hern, D. J. Durian, S. A. Langer, A. J. Liu, and S. R. Nagel, *Phys. Rev. Lett.* **89**, 095703 (2002).
- ²⁴J. Rottler and M. O. Robbins, *Phys. Rev. E* **68**, 011507 (2003).
- ²⁵F. Varnik, L. Bocquet, J. L. Barrat, and L. Berthier, *Phys. Rev. Lett.* **90**, 095702 (2003).
- ²⁶Y. Shi and M. L. Falk, *Phys. Rev. Lett.* **95**, 095502 (2005).
- ²⁷Y. Shi and M. L. Falk, *Phys. Rev. B* **73**, 214201 (2006).
- ²⁸F. Shimizu, S. Ogata, and J. Li, *Acta Mater.* **54**, 4293 (2006).
- ²⁹F. Shimizu, S. Ogata, and J. Li, *Mater. Trans.* **48**, 2923 (2007).
- ³⁰T. K. Haxton and A. J. Liu, *Phys. Rev. Lett.* **99**, 195701 (2007).
- ³¹A. S. Argon and H. Y. Kuo, *J. Non-Cryst. Solids* **37**, 241 (1980).
- ³²L. Struik, *Physical Aging in Amorphous Polymers and Other Materials* (Elsevier, Amsterdam, 1978).
- ³³D. L. Wales, *Energy Landscapes* (Cambridge University Press, Cambridge, 2003).
- ³⁴F. H. Stillinger and T. A. Weber, *Science* **225**, 983 (1984).
- ³⁵S. G. Mayr, *Phys. Rev. Lett.* **97**, 195501 (2006).
- ³⁶F. Delogu, *Phys. Rev. Lett.* **100**, 255901 (2008).
- ³⁷A. Laio and M. Parrinello, *Proc. Natl. Acad. Sci. U.S.A.* **99**, 12562 (2002).
- ³⁸A. Kushima, X. Lin, J. Li, J. Eapen, J. C. Mauro, X. Qian, P. Diep, and S. Yip, *J. Chem. Phys.* **130**, 224504 (2009).
- ³⁹C. Cerjan and W. Miller, *J. Chem. Phys.* **75**, 2800 (1981).
- ⁴⁰G. Henkelman and H. Jonsson, *J. Chem. Phys.* **111**, 7010 (1999).
- ⁴¹L. J. Munro and D. J. Wales, *Phys. Rev. B* **59**, 3969 (1999).
- ⁴²G. T. Barkema and N. Mousseau, *Phys. Rev. Lett.* **77**, 4358

- (1996).
- ⁴³N. Mousseau and G. T. Barkema, *Phys. Rev. E* **57**, 2419 (1998).
- ⁴⁴N. Mousseau and G. T. Barkema, *Phys. Rev. B* **61**, 1898 (2000).
- ⁴⁵R. Malek and N. Mousseau, *Phys. Rev. E* **62**, 7723 (2000).
- ⁴⁶D. Rodney and C. Schuh, *Phys. Rev. Lett.* **102**, 235503 (2009).
- ⁴⁷C. A. Schuh and A. C. Lund, *Nat. Mater.* **2**, 449 (2003).
- ⁴⁸A. C. Lund and C. A. Schuh, *Acta Mater.* **51**, 5399 (2003).
- ⁴⁹A. W. Lees and S. F. Edwards, *J. Phys. C* **5**, 1921 (1972).
- ⁵⁰J. Li, *Model. Simul. Mater. Sci. Eng.* **11**, 173 (2003).
- ⁵¹M. Parrinello and A. Rahman, *Phys. Rev. Lett.* **45**, 1196 (1980).
- ⁵²M. P. Allen and D. Tildesley, *Computer Simulation of Liquids* (Clarendon Press, Oxford, 1987).
- ⁵³E. Bitzek, P. Koskinen, F. Gähler, M. Moseler, and P. Gumbsch, *Phys. Rev. Lett.* **97**, 170201 (2006).
- ⁵⁴C. Lanczos, *Applied Analysis* (Dover, New York, 1988).
- ⁵⁵E. Cancès, F. Legoll, M. C. Marinica, K. Minoukadeh, and F. Willaime, *J. Chem. Phys.* **130**, 114711 (2009).
- ⁵⁶F. Valiquette and N. Mousseau, *Phys. Rev. B* **68**, 125209 (2003).
- ⁵⁷A. J. Liu and S. R. Nagel, *Nature (London)* **396**, 21 (1998).
- ⁵⁸A. S. Argon, *Acta Mater.* **27**, 47 (1979).
- ⁵⁹E. I. Corwin, H. M. Jaeger, and S. R. Nagel, *Nature (London)* **435**, 1075 (2005).
- ⁶⁰E. I. Corwin, E. T. Hoke, H. M. Jaeger, and S. R. Nagel, *Phys. Rev. E* **77**, 061308 (2008).
- ⁶¹V. Trappe, V. Prasad, L. Cipelletti, P. N. Segre, and D. A. Weitz, *Nature (London)* **411**, 772 (2001).
- ⁶²M. Cloitre, R. Borrega, F. Monti, and L. Leibler, *Phys. Rev. Lett.* **90**, 068303 (2003).
- ⁶³D. S. Grebenkov, M. P. Ciamarra, M. Nicodemi, and A. Coniglio, *Phys. Rev. Lett.* **100**, 078001 (2008).
- ⁶⁴P. G. Debenedetti and F. H. Stillinger, *Nature (London)* **410**, 259 (2001).
- ⁶⁵C. L. Rountree, D. Vandembroucq, M. Talamali, E. Bouchaud, and S. Roux, *Phys. Rev. Lett.* **102**, 195501 (2009).
- ⁶⁶M. Cloitre, R. Borrega, and L. Leibler, *Phys. Rev. Lett.* **85**, 4819 (2000).
- ⁶⁷V. Viasnoff and F. Lequeux, *Phys. Rev. Lett.* **89**, 065701 (2002).
- ⁶⁸N. R. Hansen and H. L. Schreyer, *Int. J. Solids Struct.* **31**, 359 (1994).